Nonlinear Analysis: Modelling and Control, 2009, Vol. 14, No. 1, 27–40

MHD Flow of a Micropolar Fluid past a Stretched Permeable Surface with Heat Generation or Absorption

M.-E. M. Khedr, A. J. Chamkha, M. Bayomi

Manufacturing Engineering Department
The Public Authority for Applied Education and Training
P. O. Box 42325, Shuweikh, 70654 Kuwait
achamkha@yahoo.com

Received: 2008-07-06 **Revised:** 2008-09-02 **Published online:** 2009-03-10

Abstract. This work considers steady, laminar, MHD flow of a micropolar fluid past a stretched semi-infinite, vertical and permeable surface in the presence of temperature-dependent heat generation or absorption, magnetic field and thermal radiation effects. A set of similarity parameters is employed to convert the governing partial differential equations into ordinary differential equations. The obtained self-similar equations are solved numerically by an efficient implicit, iterative, finite-difference method. The obtained results are checked against previously published work for special cases of the problem in order to access the accuarcy of the numerical method and found to be in excellent agreement. A parametric study illustrating the influence of the various physical parameters on the skin friction coefficient, microrotaion coefficient or wall couple stress as well as the wall heat transfer coefficient or Nusselt number is conducted. The obtained results are presented graphically and in tabular form and the physical aspects of the problem are discussed.

Keywords: MHD flow, micropolar fluid, stretched surface, heat generation or absorption.

Nomenclature

$B(x)$	magnetic induction	K^*	vortex viscosity
C_f	skin-friction coefficient	k^*	mean absorption coefficient
C_q	heat transfer coefficient or Nusselt number	N	angular velocity or microrotation
		N_r	radiation parameter
C_r	wall couple stress	Pr	Prandtl number
c_p	specific heat at constant pressure	$Q(x)$	heat generation or absorption coefficient
Ec	Eckert number		
f	dimensionless stream function	q_r	radiative heat flux
F_0	dimensionless wall mass transfer coefficient	T	temperature at any point
		T_w	wall temperature
Ha	Hartmann number	T_∞	free stream temperature
j	microrotation per unit mass	u	tangential or x-component of velocity

U_0	stretching velocity	w	dimensionless angular velocity or microrotation
v	normal or y-component of velocity	x	distance along the plate
V_w	dimensional wall mass transfer or suction/injection velocity	y	distance normal to the plate

Greek symbols

Δ	microrotation coupling constant	μ	fluid dynamic viscosity
α	molecular thermal diffusivity	ν	fluid apparent kinematic viscosity
ϕ	dimensionless heat generation or absorption parameter	ψ	stream function
		σ	fluid electrical conductivity
γ	spin gradient viscosity	σ^*	Stefan-Boltzmann constant
η	dimensionless distance normal to the plate	θ	dimensionless temperature
		ρ	fluid density
λ	microrotation material parameter		

1 Introduction

Micropolar fluids are referred to those fluids that contain micro-constituents that can undergo rotation which affect the hydrodynamics of the flow. In this context, they can be distinctly non-Newtonian in nature. The basic continuum theory for this class of fluids was originally formulated by Eringen [1]. The equations governing the flow of a micropolar fluid involve a microrotation vector and a gyration parameter in addition to the classical velocity vector field. Eringen's micropolar fluid theory has been employed to study a number of various flow situations such as the flow of low concentration suspensions, liquid crystals, blood, and turbulent shear flows. The theory may also be applied to explain the flow of colloidal solutions, fluids with additives and many other situations.

Over the years, the dynamics of micropolar fluids has been a popular area of research and a significant amount of research papers dealing with micropolar fluid flow over a flat plate was reported. For instance, Peddieson and McNitt [2] studied the boundary layer flow of a micropolar fluid past a semi-infinite plate. Gorla [3] investigated the forced convective heat transfer to a micropolar fluid flow over a flat plate. Rees and Bassom [4] analyzed Blasius boundary-layer flow of a micropolar fluid over a flat plate. Hady [5] considered heat transfer to micropolar fluid from a non-isothermal stretching sheet with injection. Kelson and Desseaux [6] studied the effect of surface conditions on the flow of a micropolar fluid driven by a porous stretching surface. The boundary layer flow of micropolar fluids past a semi-infinite plate was studied by Ahmadi [7] taking into account the gyration vector normal to the xy-plane and the micro-inertia effects. Soundalgekar and Takhar [8] studied the flow and heat transfer of a micropolar fluid past a continuously moving plate. Perdikis and Raptis [9] studied the heat transfer of a micropolar fluid in the presence of radiation and later Raptis [10] considered the flow of a micropolar fluid past a continuously moving plate in the presence of radiation. El-Arabawy [11] analyzed the problem of the effect of suction/injection on the flow of a micropolar fluid past a continuously moving plate in the presence of radiation. Abo-

Eldahab and Ghonaim [12] studied radiation effects on heat transfer of a micropolar fluid through a porous medium. Abo-Eldahab and El Aziz [13] analyzed flow and heat transfer in a micropolar fluid past a stretching surface embedded in a non-Darcian porous medium with uniform free stream. Eldabe and Ouaf [14] solved the problem of heat and mass transfer in a hydromagnetic flow of a micropolar fluid past a stretching surface with Ohmic heating and viscous dissipation using the Chebyshev finite difference method. Odda and Farhan [15] studied the effects of variable viscosity and variable thermal conductivity on heat transfer to a micro-polar fluid from a non-isothermal stretching sheet with suction and blowing. Mahmoud [16] considered thermal radiation effects on MHD flow of a micropolar fluid over a stretching surface with variable thermal conductivity. Aouadi [17] reported a numerical study for micropolar flow over a stretching sheet.

In certain applications such as those involving heat removal from nuclear fuel debris, underground disposal of radioactive waste material, storage of food stuffs, and exothermic chemical reactions and dissociating fluids in packed-bed reactors, the working fluid heat generation or absorption effects are important. Patil and Kulkarni [18] studied the effects of chemical reaction on free convective flow of a polar fluid through a porous medium in the presence of internal heat generation. Representative studies dealing with heat generation or absorption effects have been reported previously by such authors as Acharya and Goldstein [19], Vajravelu and Nayfeh [20] and Chamkha [21].

The objective of this paper is to consider MHD flow of a micropolar fluid along a vertical semi-infinite permeable plate in the presence of wall suction or injection effects and heat generation or absorption effects.

2 Problem formulation

Consider steady, laminar, MHD boundary-layer flow of a micropolar fluid past a permeable uniformly stretched semi-infinite vertical plate in the presence of heat generation or absorption, thermal radiation and viscous dissipation effects. The fluid is assumed to be viscous and has constant properties. The applied magnetic field is assumed to be constant and the magnetic Reynolds number is assumed to be small so that the induced magnetic field is neglected. No electric field is assumed to exist and the Hall effect of magnetohydrodynamics is neglected.

The governing boundary-layer equations may be written as follows:

$$\frac{\partial u}{\partial x} + \frac{\partial v}{\partial y} = 0, \tag{1}$$

$$u\frac{\partial u}{\partial x} + v\frac{\partial u}{\partial y} = \frac{\mu + K^*}{\rho}\frac{\partial^2 u}{\partial y^2} + \frac{K^*}{\rho}\frac{\partial N}{\partial y} - \frac{\sigma B^2(x)}{\rho}u, \tag{2}$$

$$\frac{\gamma}{K^*}\frac{\partial^2 N}{\partial y^2} - 2N - \frac{\partial u}{\partial y} = 0, \tag{3}$$

$$u\frac{\partial T}{\partial x} + v\frac{\partial T}{\partial y} = \alpha\frac{\partial^2 T}{\partial y^2} + \frac{\nu}{c_p}\left(\frac{\partial u}{\partial y}\right)^2 + \frac{Q(x)}{\rho c_p}(T - T_\infty) - \frac{1}{\rho c_p}\frac{\partial q_r}{\partial y}, \tag{4}$$

where u, v, N, and T are the fluid x-component of velocity, y-component of velocity, angular velocity or microrotation and temperature, respectively. ρ, ν ($\nu = (\mu + K^*)/\rho$), μ, c_p and α are the fluid density, apparent kinematic viscosity, fluid dynamic viscosity, specific heat at constant pressure and thermal diffusivity, respectively. γ and K^* are the spin gradient viscosity and the vortex viscosity, respectively. $\sigma, B(x), Q(x)$ and q_r are the electrical conductivity, magnetic induction, heat generation (> 0) or absorption (< 0) coefficient and the radiative heat flux, respectively.

The boundary conditions for this problem can be written as

$$y = 0: \quad u = U_0, \quad v = V_w, \quad N = 0, \quad T = T_w, \tag{5}$$

$$y \to \infty: \quad u \to 0, \quad N \to 0, \quad T \to T_\infty, \tag{6}$$

where U_0, V_w and T_w are the stretching velocity, suction ($V_w < 0$) or injection ($V_w > 0$) velocity and wall temperature, respectively.

By using Rosseland approximation and following El-Arabawy [11], the radiative heat flux q_r is given by

$$q_r = -\frac{4\sigma^*}{3k^*}\frac{\partial(T^4)}{\partial y}, \tag{7}$$

where σ^* is the Stefan-Boltzmann constant and k^* is the mean absorption coefficient.

Assuming that the temperature differences within the flow are sufficiently small so that T^4 can be expanded in Taylor series about the free stream temperature T_∞ to yield

$$T^4 \equiv 4T_\infty^3 T - 3T_\infty^4, \tag{8}$$

where the higher-order terms of the expansion are neglected.

Defining the dimensional stream function in the usual way such that $u = \frac{\partial \psi}{\partial y}$ and $v = -\frac{\partial \psi}{\partial x}$ and using the following dimensionless variables (El-Arabawy, [11]):

$$\begin{aligned} &\eta = y\sqrt{\frac{U_0}{2\nu x}}, && \psi = \sqrt{2\nu U_0 x f(\eta)}, \\ &\theta(\eta) = \frac{T - T_\infty}{T_w - T_\infty}, && N = \sqrt{\frac{U_0^3}{2\nu x}}w(\eta), \\ &u = U_0 f'(\eta), && v = -\sqrt{\frac{\nu U_0}{2x}}[t(\eta) - \eta f'(\eta)]. \end{aligned} \tag{9}$$

Along with equations (7) and (8) results in the following self-similar equations:

$$f''' + ff'' - Ha^2 f' + \Delta w' = 0, \tag{10}$$

$$\lambda w'' - 4w - 2f'' = 0, \tag{11}$$

$$(3N_r + 4)\theta'' + 3N_r Pr f\theta' + 3N_r Pr\,\phi\,\theta + 3N_r PrEc(f'')^2 = 0, \tag{12}$$

where

$$Ha = \sqrt{\frac{2\sigma x B^2(x)}{\rho U_0}}, \quad Pr = \frac{\rho\nu c_p}{k}, \quad \lambda = \frac{\gamma U_0}{K^*\nu x}, \quad \Delta = \frac{K^*}{\rho\nu},$$
$$Ec = \frac{U_0^2}{c_p(T_w - T_\infty)}, \quad \phi = \frac{2xQ(x)}{\rho c_p U_0}, \quad N_r = \frac{\kappa k^*}{4\sigma^* T_\infty^3} \tag{13}$$

are the Hartmann number, Prandtl number, microrotation parameter, coupling constant parameter, Eckert number, dimensionless internal heat generation or absorption parameter and the radiation parameter, respectively. It should be noted that $B(x) = B_0/x^{1/2}, \gamma(x) = \gamma_0 x$ and $Q(x) = Q_0/x$ where B_0, γ_0 and Q_0 are constants.

The dimensionless form of the boundary conditions becomes

$$\eta = 0: \quad f = F_0, \quad f' = 1, \quad w = 0, \quad \theta = 1, \tag{14}$$
$$\eta \to \infty: \quad f' \to 0, \quad w \to 0, \quad \theta \to 0, \tag{15}$$

where $F_0 = -V_w/\sqrt{2x/(\nu U_0)}$ is the dimensionless suction of injection velocity such that $F_0 > 0$ indicates fluid wall suction and $F_0 < 0$ indicates fluid wall blowing or injection.

The local skin-friction coefficient, wall couple stress and the local heat transfer (or Nusselt number) coefficients are important physical parameters for this flow and heat transfer situation. These are defined as follows:

$$C_f = \frac{(\mu + K^*)(\partial u/\partial y)_{y=0} + K^* N|_{y=0}}{(1/2)\rho U_0^2} = -2Re_x^{-(1/2)} f''(0), \tag{16}$$

$$C_r = \frac{(\gamma/K^*)(\partial N/\partial y)_{y=0}}{\gamma U_0^3 (2K^*\nu^2)} = Re_x^{-1} w'(0), \tag{17}$$

$$C_q = \frac{-x(\partial T/\partial y)_{y=0}}{T_w - T_\infty} = -2Re_x^{-(1/2)}\theta'(0), \tag{18}$$

where $Re_x = U_0 x/\nu$ is the local Reynolds number.

3 Numerical method

The implicit finite-difference method discussed by Blottner [22] has proven to be adequate and accurate for the solution of differential equations similar to equations (10) through (11). For this reason, it is employed in the present work. These equations have been linearized and then descritized using three-point central difference quotients with variable step sizes in the η direction. The resulting equations form a tri-diagonal system of algebraic equations that can be solved line by line by the well-known Thomas algorithm (see Blottner, [22]). Due to the nonlinearities of the equations, an iterative solution is required. For convergence, the maximum absolute error between two successive iterations was taken to be 10^{-7}. A starting step size of 0.001 in the η direction with an increase of 1.0375 times the previous step size was found to give accurate results. The total number of points in η direction was taken to be 199.

The accuracy of the aforementioned numerical method was validated by direct comparisons with the numerical results reported earlier by El-Arabawy [11]. Tables 1 and 2 present comparisons for the wall slopes of velocity, microrotation and temperature values for various conditions. These comparisons show excellent agreement between the results.

Table 1. Comparison of $-f''(0)$ and $w'(0)$ with El-Arabawy [11] for $Ha = 0$, $\Delta = 0.2$ and $\lambda = 2.0$

F_0	$-f''(0)$ El-Arabawy [11]	$w'(0)$ El-Arabawy [11]	$-f''(0)$ Present Work	$w'(0)$ Present Work
-0.7	0.278827	0.236917	0.278939	0.237101
-0.4	0.404227	0.286997	0.404381	0.287120
-0.2	0.504059	0.321165	0.504192	0.321321
0	0.616542	0.355330	0.616844	0.355563
0.2	0.741521	0.389278	0.741691	0.389410
0.4	0.877517	0.422223	0.877682	0.422393
0.7	1.099430	0.468923	1.103311	0.469098

Table 2. Comparison of $-\theta'(0)$ with El-Arabawy [11] for $Ec = 0.02$, $F_0 = 0$, $Ha = 0$, $N_r = \infty$, $\Delta = 0.2$, $\lambda = 2.0$ and $\Phi = 0$

Pr	$-\theta'(0)$ El-Arabawy [11]	$-\theta'(0)$ Present Work
0.733	0.501327	0.501423
7.0	1.931150	1.931256
10	2.337000	2.337201
20	3.360750	3.360839
50	5.380040	5.380149

4 Results and discussion

Figs. 1 through 3 display the influence of the Hartmann number Ha on the velocity (f'), microrotation (w) and the temperature (θ) profiles. The presence of a magnetic field has the tendency to produce a drag-like force called the Lorentz force which acts in the opposite direction of the fluid's motion. This causes the fluid velocity and microrotation to decrease and the fluid temperature to increase as the Hartmann number Ha increases. In addition, the boundary-layer thickness decreases while the thermal boundary-layer thickness increases as Ha increases. It is also observed from Fig. 2 that as Ha increases, the microrotation decreases everywhere within the boundary layer except in the immediate vicinity of the plate surface.

Table 3 illustrates the effects of the Hartmann number Ha on the skin-friction coefficient ($-f''(0)$), the wall couple stress ($w'(0)$) and the Nusselt number ($-\theta'(0)$). As mentioned before, increasing the value of Ha causes the linear velocity to decrease resul-

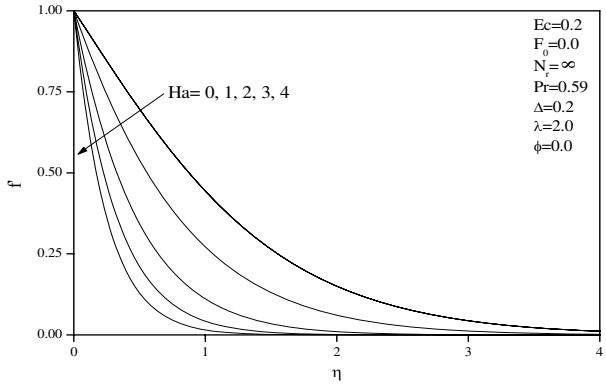

Fig. 1. Effects of Ha on velocity profiles.

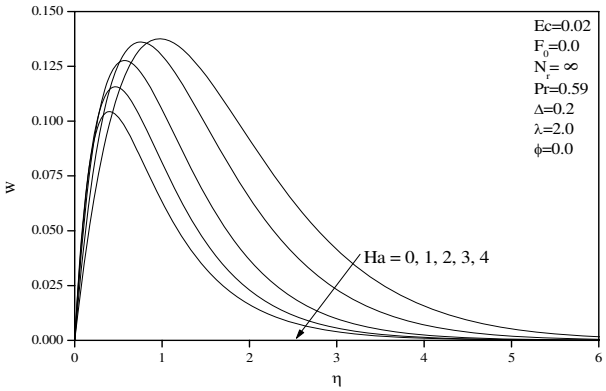

Fig. 2. Effects of Ha on angular velocity profiles.

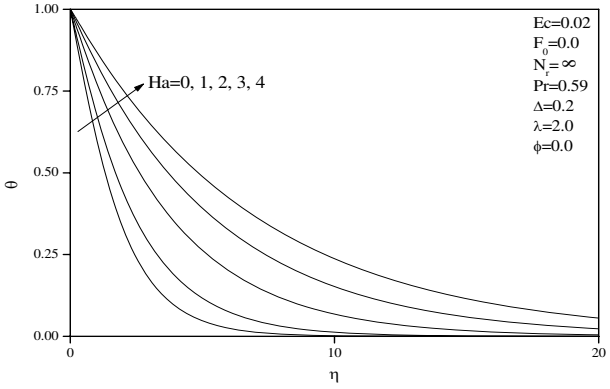

Fig. 3. Effects of Ha on temperature profiles.

ting in increased negative wall slope of the velocity ($-f''(0)$). Similarly, the wall slope of the microrotation or angular velocity increases as Ha increases. On the other hand, it is also observed that the negative wall slope of the temperature profile ($-\theta'(0)$) or the Nusselt number decreases as Ha increases.

Table 3. Effects of Ha on $-f''(0)$, $w'(0)$ and $-\theta'(0)$ for $Ec = 0.02$, $F_0 = 0$, $N_r = \infty$, $Pr = 0.59$, $\Delta = 0.2$, $\lambda = 2.0$ and $\phi = 0$

Ha	$-f''(0)$	$w'(0)$	$-\theta'(0)$
0	0.6168441	0.3555639	0.4301508
1	1.14692	0.4715558	0.3418584
2	2.066495	0.6029878	0.2310590
3	3.040321	0.6871593	0.1609032
4	4.028647	0.7429327	0.1159298

Figs. 4 through 6 show representative velocity, microrotation and temperature profiles for various values of the wall mass transfer parameter F_0, respectively. In general, imposition of fluid wall suction ($F_0 > 0$) tends to decrease all of the fluid velocity, microrotation, and temperature as well as their boundary-layer thicknesses. On the other hand, injection or blowing of fluid at the plate surface ($F_0 < 0$) produces the exact opposite effect namely increases in the fluid velocity, microrotation and temperature and their boundary-layer thicknesses. These behaviors are obvious from Figs. 4 through 6. In addition, it is seen from Fig. 5 that as F_0 increases, the angular velocity or microrotaion increases close to the plate surface and then decreases elsewhere.

Table 4 depicts the influence of the wall mass transfer parameter F_0 on the skin-friction coefficient, the wall couple stress and the Nusselt number. Increasing the value of F_0 from negative to positive values causes increases in all of the negative wall slopes of the velocity and temperature and the wall slope of the angular velocity or microrotation resulting in increased values of all of the skin-friction coefficient, the wall couple stress and the Nusselt number. These behaviors are clear from Table 4.

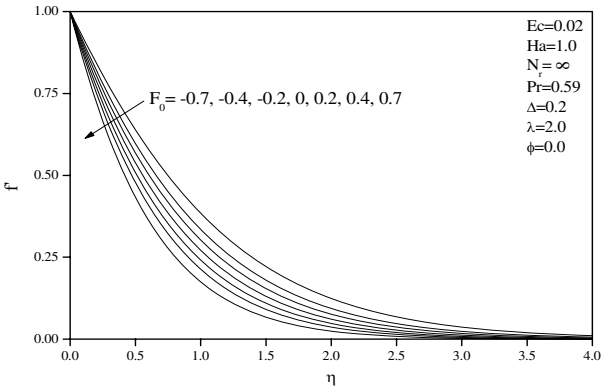

Fig. 4. Effects of F_0 on velocity profiles.

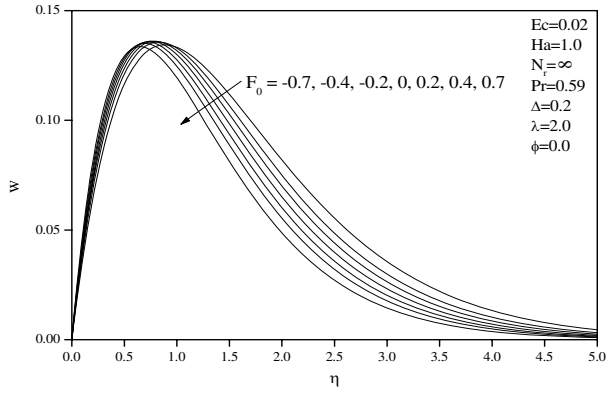

Fig. 5. Effects of F_0 on angular velocity profiles.

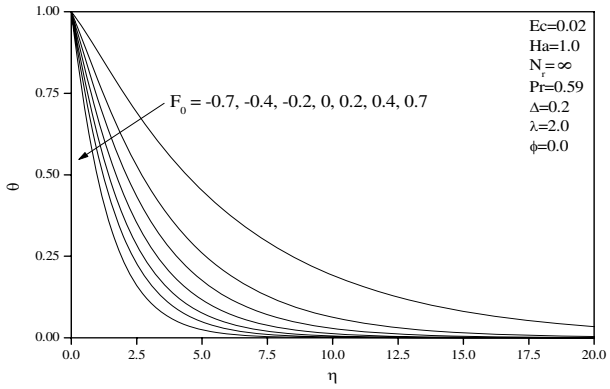

Fig. 6. Effects of F_0 on temperature profiles.

Table 4. Effects of F_0 on $-f''(0),\ w'(0)$ and $-\theta'(0)$ for $Ec = 0.02,\ Ha = 1.0,$ $N_r = \infty,\ Pr = 0.59,\ \Delta = 0.2,\ \lambda = 2.0$ and $\phi = 0$

F_0	$-f''(0)$	$w'(0)$	$-\theta'(0)$
-0.7	0.8197412	0.3964357	0.1032472
-0.4	0.9477000	0.4284665	0.1947786
-0.2	1.043334	0.4500362	0.2649712
0	1.146929	0.4715558	0.3418584
0.2	1.258714	0.4928372	0.4244762
0.4	1.378121	0.5136983	0.5113263
0.7	1.571476	0.5439026	0.6493271

Fig. 7 presents the effect of the Prandtl number Pr on the temperature profiles. Increasing the value of Pr has the tendency to decrease the fluid temperature in the boundary layer as well as the thermal boundary-layer thickness. This causes the wall slope of the temperature profile to decrease as Pr increases causing the Nusselt number to increase as clearly seen from Table 5. From Table 5, it is also observed that the skin-friction coefficient and the wall couple stress do not change as Pr changes. This is expected since the linear and angular momentum equations (8) and (9) are uncoupled from the energy equation (10) for this problem.

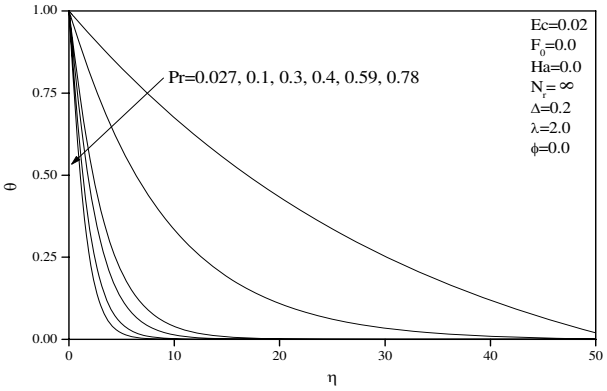

Fig. 7. Effects of Pr on temperature profiles.

Table 5. Effects of Pr on $-f''(0)$, $w'(0)$ and $-\theta'(0)$ for $Ec = 0.02$, $F_0 = 0$, $Ha = 0$, $N_r = \infty$, $\Delta = 0.2$, $\lambda = 2.0$ and $\phi = 0$

Pr	$-f''(0)$	$w'(0)$	$-\theta'(0)$
0.027	0.6168441	0.3555639	0.0367856
0.1	0.6168441	0.3555639	0.0997646
0.3	0.6168441	0.3555639	0.2570476
0.4	0.6168441	0.3555639	0.3219283
0.59	0.6168441	0.3555639	0.4301508
0.78	0.6168441	0.3555639	0.5230769

Fig. 8 presents the temperature profile for various values of the heat generation or absorption coefficient ϕ. In general, the presence of heat generation effects ($\phi > 0$) has the tendency to increase the temperature of the fluid. It is also interesting to note that for $\phi = 1.0$ a distinctive peak in the temperature profile greater than that of the wall occurs in the vicinity of the plate surface. However, the case when $\phi = 2.0$ does not follow the same increasing trend as it drops below the profile for $\phi = 1.0$ with a noted oscillatory behavior. On the other hand, the opposite behavior in the temperature profiles is obtained due to the presence of heat absorption effects ($\phi < 0$). The peak temperature value in the case of heat absorption is that of the wall. All of these trends are clearly seen from Fig. 8.

The variations of the skin-friction coefficient, the wall couple stress and the Nusselt number as ϕ changes is shown in Table 6. As expected the values of $-f''(0)$ and $w'(0)$ do not change as ϕ changes. This is because the energy equation is uncoupled from the momentum equations. However, the values of $-\theta'(0)$ follow a consistent decreasing trend for heat absorption conditions as increases from -2 to 0 (no heat source or sink). On the other hand, in general, for heat generation, the Nusselt number decreases as ϕ increases but the value $-\theta'(0)$ for $\phi = 2.0$ is higher than that for $\phi = 1.0$. It is also predicted that the Nusselt number becomes negative $\phi = 1$. This is associated with the existence of the peak in the temperature profiles for $\phi = 1$ (see Fig. 8) which causes its wall slope to change its sign.

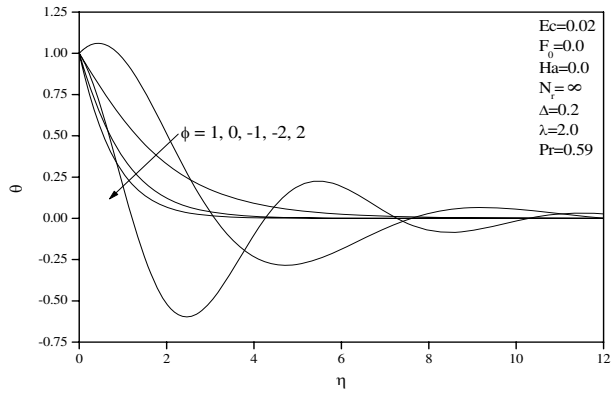

Fig. 8. Effects of ϕ on temperature profiles.

Table 6. Effects of ϕ on $-f''(0)$, $w'(0)$ and $-\theta'(0)$ for $Ec = 0.02$, $F_0 = 0$, $Ha = 0$, $N_r = \infty$, $Pr = 0.59$, $\Delta = 0.2$ and $\lambda = 2.0$

ϕ	$-f''(0)$	$w'(0)$	$-\theta'(0)$
-2	0.6168441	0.3555639	1.188622
-1	0.6168441	0.3555639	0.9009093
0	0.6168441	0.3555639	0.4301508
1	0.6168441	0.3555639	-0.2990513
2	0.6168441	0.3555639	0.3488447

In Table 7, the influence of the radiation parameter N_r on the values of $-f''(0)$, $w'(0)$ and $-\theta'(0)$ is shown. Again, since the energy equation is uncoupled from the momentum equations, the values of $-f''(0)$ and $w'(0)$ do not change as N_r changes. However, the values of $-\theta'(0)$ increase as N_r increases. It should be noted that the case $N_r = \infty$ correspond to the condition where thermal radiation effect is absent. This indicates that as the parameter N_r increases, thermal radiation effects become lower and this means that the temperature decreases and the negative slope of the temperature profile at the surface increases resulting in increased heat transfer or Nusselt number values.

Thus, the conclusion here is that the addition of the thermal radiation effect in the model, results in increases in the fluid temperature and reductions in the Nusselt number.

Table 8 elucidates the effect of increasing the value of the microrotation coupling constant Δ on the values of $-f''(0)$ and $w'(0)$ and $-\theta'(0)$. It is predicted that as Δ increases, the values of $-f''(0)$ and $-\theta'(0)$ decrease while the values of $w'(0)$ increase.

Table 7. Effects of N_r on $-f''(0)$, $w'(0)$ and $-\theta'(0)$ for $Ec = 0.02$, $F_0 = 0$, $Ha = 1.0$, $Pr = 0.59$, $\Delta = 0.2$, $\lambda = 2.0$ and $\phi = 0$

N_r	$-f''(0)$	$w'(0)$	$-\theta'(0)$
0.1	1.146929	0.4715558	0.0372252
0.5	1.146929	0.4715558	0.1103665
1.0	1.146929	0.4715558	0.1659859
2.0	1.146929	0.4715558	0.2232631
3.0	1.146929	0.4715558	0.2523357
5.0	1.146929	0.4715558	0.2815142
10	1.146929	0.4715558	0.3089046
∞	1.146929	0.4715558	0.3418584

Table 8. Effects of Δ on $-f''(0)$, $w'(0)$ and $-\theta'(0)$ for $Ec = 0.02$, $F_0 = 0$, $Ha = 1.0$, $N_r = \infty$, $Pr = 0.59$, $\lambda = 2.0$ and $\phi = 0$

Δ	$-f''(0)$	$w'(0)$	$-\theta'(0)$
0	1.163697	0.4706068	0.3445972
0.1	1.155352	0.4710780	0.3433341
0.2	1.146929	0.4715558	0.3418584
0.3	1.138881	0.4720554	0.3405513
0.4	1.130228	0.4725627	0.3392475
0.5	1.121886	0.4730935	0.3376332

5 Conclusions

The problem of steady, laminar, boundary-layer flow of a viscous, micropolar and heat generating or absorbing fluid past a vertical uniformly stretched permeable plate was considered. The governing equations for this problem were developed and transformed using appropriate similarity transformations. The resulting similarity equations were then solved numerically by an implicit, iterative, finite-difference scheme. The obtained results for special cases of the problem were compared with previously published work and found to be in excellent agreement. It was found that, in general, the local skin-friction coefficient increased as either of the wall suction or injection parameter or the Hartmann number increased while it decreased as the microrotation coupling constant increased. In addition, the local heat transfer coefficient or Nusslet number was predicted to increase due to increases in either of the suction or injection parameter, Prandtl number or the radiation parameter while it decreased as either of the Hartmann number, the heat generation

or absorption coefficient or the microrotation coupling constant increased. Finally, the local wall microrotation coefficient or couple stress was increased as either of the wall suction or injection parameter, Hartmann number or the microrotation coupling constant increased. It is hoped that the present work will serve as a vehicle for understanding more complex problems involving the various physical effects investigated in the present problem.

Acknowledgement

The authors acknowledge and appreciate the financial support of this work by the Public Authority for Applied Education & Training under Project No. TS-07-15.

References

1. A. C. Eringen, Theory of micropolar fluids, *J. Math. Mech.*, **16**, pp. 1–18, 1966.
2. J. Peddieson, R. P. McNitt, Boundary layer theory for micropolar fluid, *Recent Adv. Eng. Sci.*, **5**, pp. 405–426, 1970.
3. R. S. R. Gorla, Heat transfer in micropolar boundary layer flow over a flat plate, *Int. J. Eng. Sci.*, **21**, pp. 791–796, 1983.
4. D. A. S. Rees, A. P. Bassom, The Blasius boundary-layer flow of a micropolar fluid, *Int. J. Eng. Sci.*, **34**, pp. 113–124, 1996.
5. F. M. Hady, On the heat transfer to micropolar fluid from a non-isothermal stretching sheet with injection, *Int. J. Num. Meth. Heat Fluid Flow*, **6**, pp. 99–104, 1996.
6. N. A. Kelson, A. Desseaux, Effects of surface conditions on flow of a micropolar fluid driven by a porous stretching sheet, *Int. J. Eng. Sci.*, **39**, pp. 1881–1897, 2001.
7. G. Ahmadi, Self-similar solution of incompressible micropolar boundary layer flow over a semi-infinite plate, *Int. J. Eng. Sci.*, **14**, pp. 639–646, 1976.
8. V. M. Soundalgekar, H. S. Takhar, Flow of a micropolar fluid on a continuous moving plate, *Int. J. Eng. Sci.*, **21**, pp. 961–965, 1983.
9. C. Perdikis, A. Raptis, Heat transfer of a micropolar fluid by the presence of radiation, *Heat Mass Transfer*, **31**, pp. 381–382, 1996.
10. A. Raptis, Flow of a micropolar fluid past a continuously moving plate by the presence of radiation, *Int. J. Heat Mass Tran.*, **41**, pp. 2865–2866, 1998.
11. H. A. M. El-Arabawy, Effect of suction/injection on the flow of a micropolar fluid past a continuously moving plate in the presence of radiation, *Int. J. Heat Mass Tran.*, **46**, pp. 1471–1477, 2003.
12. E. M. Abo-Eldahab, A. F. Ghonaim, Radiation effect on heat transfer of a micropolar fluid through a porous medium, *Appl. Math. Comput.*, **169**, pp. 500–510, 2005.

13. E. M. Abo-Eldahab, M. A. El Aziz, Flow and heat transfer in a micropolar fluid past a stretching surface embedded in a non-Darcian porous medium with uniform free stream, *Appl. Math. Comput.*, **162**, pp. 881–899, 2005.

14. N. T. Eldabe, M. E. M. Ouaf, Chebyshev finite difference method for heat and mass transfer in a hydromagnetic flow of a micropolar fluid past a stretching surface with Ohmic heating and viscous dissipation, *Appl. Math. Comput.*, **177**, pp. 561–571, 2006.

15. S. N. Odda, A. M. Farhan, Chebyshev finite difference method for the effects of variable viscosity and variable thermal conductivity on heat transfer to a micro-polar fluid from a non-isothermal stretching sheet with suction and blowing, *Chaos Soliton. Fract.*, **30**, pp. 851–858, 2006.

16. M. A. A. Mahmoud, Thermal radiation effects on MHD flow of a micropolar fluid over a stretching surface with variable thermal conductivity, *Physica A*, **375**, pp. 401–410, 2007.

17. M. Aouadi, Numerical study for micropolar flow over a stretching sheet, *Comp. Mater. Sci.*, **38**, pp. 774–780, 2007.

18. P. M. Patil, P. S. Kulkarni, Effects of chemical reaction on free convective flow of a polar fluid through a porous medium in the presence of internal heat generation, *Int. J. Therm. Sci.*, **47**, pp. 1043–1054, 2008.

19. S. Acharya, R. J. Goldstein, Natural convection in an externally heated vertical or inclined square box containing internal energy sources, *ASME. J. Heat Transf.*, **107**, pp. 855–866, 1985.

20. K. Vajravelu, J. Nayfeh, Hydromagnetic convection at a cone and a wedge, *Int. Commun. Heat Mass*, **19**, pp. 701–710, 1992.

21. A. J. Chamkha, Non-Darcy fully developed mixed convection in a porous medium channel with heat generation/absorption and hydromagnetic effects, *Numer. Heat Transfer*, **32**, pp. 853–875, 1997.

22. F. G. Blottner, Finite-difference methods of solution of the boundary-layer equations, *AIAA J.*, **8**, pp. 93–205, 1970.